Journal of Materials Chemistry C

ROYAL SOCIETY OF CHEMISTRY

PAPER

View Article Online
View Journal | View Issue

Cite this: J. Mater. Chem. C, 2023, 11, 12941

Boosting electron transport in non-fullerene acceptors using non-chlorinated solvents†

Mohamad Insan Nugraha, ‡*[a] Ryanda Enggar Anugrah Ardhi, ‡[a] Dipti Naphade,[a] Weimin Zhang,[a] Youyou Yuan,[b] Martin Heeney[a] and Thomas D. Anthopoulos *[a]

Received 12th June 2023,
Accepted 1st September 2023

DOI: 10.1039/d3tc02037a

rsc.li/materials-c

Chlorinated solvents are commonly used to process organic semiconductor devices but have several negative environmental impacts. The choice of processing solvent significantly affects the layer microstructure and device performance, so replacing chlorinated solvents is non-trivial. Herein, we investigate the microstructural and electron-transporting properties of small-molecule non-fullerene acceptor (NFA) films and transistors processed from various non-chlorinated solvents. We show that the ensuing NFA transistors exhibit improved layer morphology, crystallinity, and electron mobility superior to those processed from chlorinated solvents. Our work highlights using non-chlorinated solvents to optimise charge transport in organic semiconductors and their devices while mitigating adverse environmental effects.

Introduction

There is increasing research interest in organic semiconductors (OSCs) owing to their potential for many current and future (opto)electronic applications.[1–8] These materials offer attractive attributes such as light weight, good mechanical flexibility, and excellent optical transparency, highlighting their compatibility with next-generation flexible electronics.[9–12] OSCs are also solution-processable, which allows functional (opto)electronic device fabrication using cost-effective and low-temperature processing methods.[13–16] Furthermore, the properties of OSCs can be controlled *via* several approaches, for instance, introducing/replacing heteroatoms and tailoring functional groups in side chains.[17,18] Among the vast library of OSCs, small-molecule non-fullerene acceptors (NFAs) attract the most interest.[19,20] NFAs offer remarkable tunability in their optical absorption and energy level characteristics, which are advantageous for the realisation of highly efficient organic photovoltaics (OPVs).[21–24]

Integrating NFAs into functional devices typically involves using chlorinated solvents to solubilise the materials before film deposition.[21,22,25] However, chlorinated solvents are among the worst in terms of their environmental impact and toxicity.[26] Therefore, using non-chlorinated solvents with lower toxicity and environmental impact is important to overcome these issues.[27–29] To this end, using non-chlorinated solvents for NFA-based thin-film transistors (TFTs) has received little attention. Solvent characteristics critically influence the material solubility and growth kinetics during film deposition, ultimately determining the optoelectronic properties of the NFA films.

Herein, we study the charge transport characteristics of NFA TFTs fabricated from various non-chlorinated solvents. We find that the choice of solvent critically influences the electronic, optical, and microstructural properties of the NFA films. We show that charge transport in the NFA TFTs can be significantly improved using non-chlorinated rather than chlorinated solvents. The field-effect mobility enhancement is correlated to the improved microstructural characteristics of the NFA layers.

Results and discussion

We selected *o*-IDTBR[30–32] and L8-BO[33] as the model NFA systems for this study (Fig. 1a). The full chemical names of the two NFAs are given in the ESI.† *O*-IDTBR is a known high-electron-mobility OSC that has been used successfully to develop high electron mobility TFTs,[34,35] whereas L8-BO has been extensively studied as one of the highest-performing NFAs for application in next-generation OPVs.[36–38] Both NFAs are commonly dissolved using chlorinated solvents such as

[a] King Abdullah University of Science and Technology (KAUST), KAUST Solar Center (KSC), Division of Physical Sciences and Engineering (PSE), Thuwal, 23955-6900, Saudi Arabia. E-mail: mohamad.nugraha@kaust.edu.sa, thomas.anthopoulos@kaust.edu.sa

[b] Imaging and Characterization Core Lab, The Physical Characterization Lab Division, KAUST, Thuwal 23955-6900, Saudi Arabia

† Electronic supplementary information (ESI) available. See DOI: https://doi.org/10.1039/d3tc02037a

‡ These authors contributed equally.

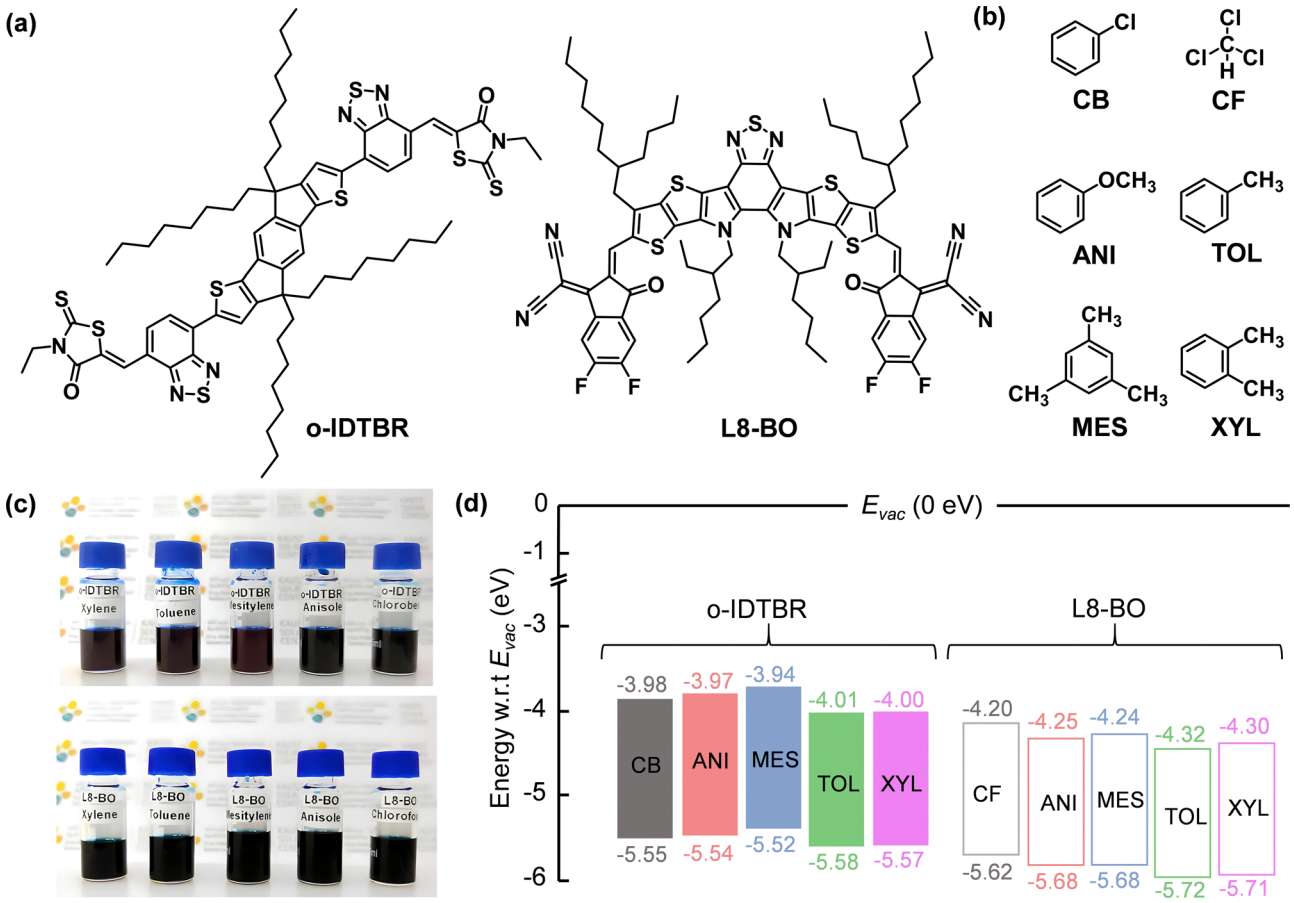

Fig. 1 (a) Molecular structures of *o*-IDTBR and L8-BO non-fullerene acceptors (NFAs) investigated in this work. (b) Chemical structures of the solvents studied in this work, including chlorobenzene (CB), chloroform (CF), anisole (ANI), mesitylene (MES), toluene (TOL), and *o*-xylene (XYL). (c) Photographs of *o*-IDTBR (top panel) and L8-BO (bottom panel) solutions in different solvents. (d) Energy level diagram of *o*-IDTBR and L8-BO processed using different solvents, obtained from photoelectron spectroscopy in air (PESA) and absorption spectroscopy measurements.

chlorobenzene (CB) and chloroform (CF), which are then used to fabricate the functional devices. For example, *O*-IDTBR yields high-performance TFTs when processed from chlorobenzene (CB) solutions, whereas L8-BO exhibits optimal charge transport when cast from chloroform (CF) solutions.[36–41] To investigate the possibility of using more eco-friendly solvents, we selected various non-chlorinated solvents, including anisole (ANI), mesitylene (MES), toluene (TOL), and *o*-xylene (XYL) (see Fig. 1b) to dissolve both NFAs.

To begin, we investigated the solubility of NFAs in different solvents. Fig. 1c displays photographs of the various NFA solutions. Both NFAs demonstrated solubility in all non-chlorinated solvents investigated, with no evidence of particle aggregates. There were no noticeable colour changes in the L8-BO solutions made using various solvents (Fig. 1c). Conversely, we observed colour changes in the *o*-IDTBR solutions, with the initial dark bluish tint transitioning to dark reddish hues when changing solvents from chlorobenzene to mesitylene, toluene, and *o*-xylene (Fig. 1c, top panel).

We also assessed the film properties of both NFAs following spin casting from various solvents. Fig. S1 (ESI†) shows photographs of the *o*-IDTBR and L8-BO NFA films after spin casting from the various solutions. The films were continuous and smooth, except for the *o*-IDTBR and L8-BO films processed from anisole. The latter films exhibit some visible non-uniformities with uncoated regions and particle aggregates. This imperfect film quality can be attributed to the limited solubility of these NFAs in anisole. Among the solvents investigated, we observed that the NFA films processed from toluene possess the most uniform and smooth properties, as depicted in Fig. S1 (ESI†).

Next, we investigated whether solvents can affect the electronic structures of NFA films, such as the highest occupied molecular orbital (HOMO) and the lowest unoccupied molecular orbital (LUMO), using photoelectron spectroscopy in air (PESA) and ultraviolet-visible (UV-Vis) absorption measurements. The HOMO and LUMO levels of the various NFA films are summarised in Fig. 1d. The HOMO level of *o*-IDTBR and L8-BO prepared from the different solvents measured using PESA measurements are depicted in Fig. S2 (ESI†). In chlorinated solvents, *o*-IDTBR and L8-BO possess HOMO levels of −5.55 and −5.62 eV, respectively. Upon dissolving *o*-IDTBR in anisole and mesitylene, we observed only a slight change in the HOMO level to −5.54 and −5.52, respectively. On the other hand,

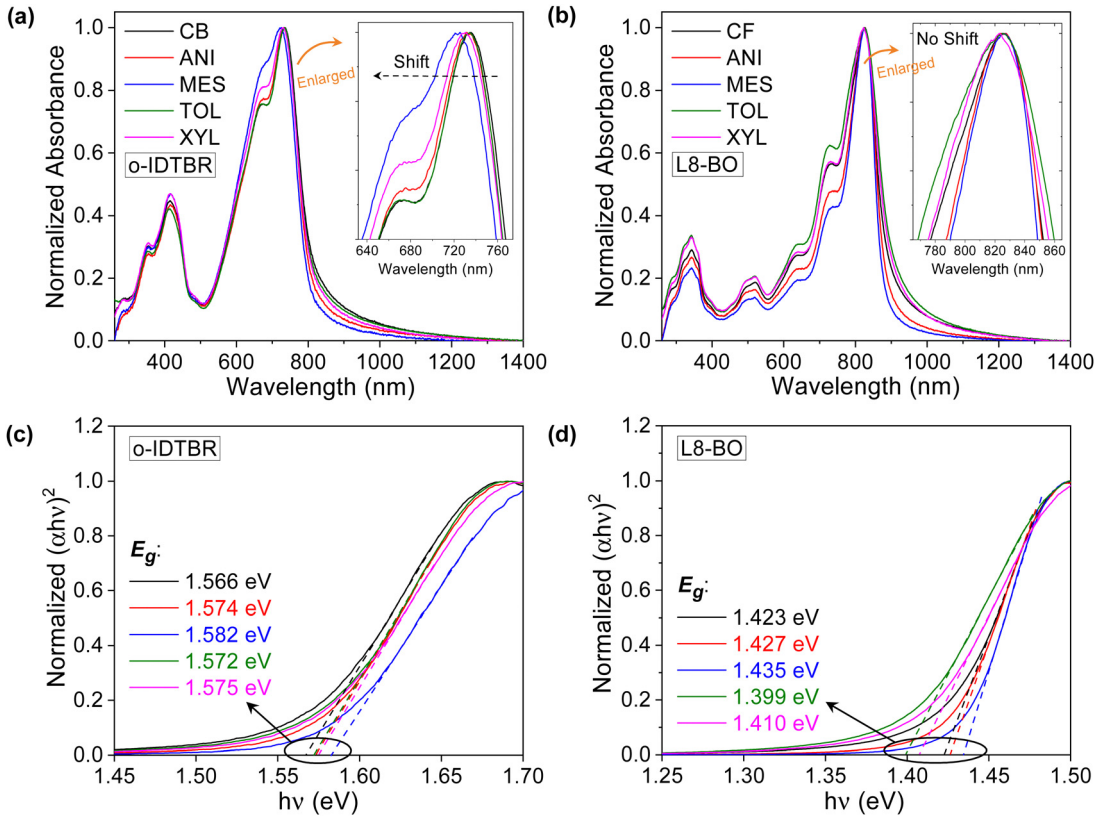

Fig. 2 Normalised absorbance of (a) *o*-IDTBR and (b) L8-BO films processed using different solvents. Tauc plot of (c) *o*-IDTBR and (d) L8-BO films processed using different solvents.

dissolving L8-BO in anisole and mesitylene results in a slightly deeper HOMO level of −5.68 eV (for both solvents). Interestingly, for both NFAs, we observed that their HOMO levels became deeper when cast from toluene and *o*-xylene solutions. The results are most likely attributed to pre-aggregation in the NFA solutions and changes in the growth kinetics during film formation when cast from toluene and *o*-xylene.[42]

The choice of solvents can significantly influence the optical, morphological, and crystallinity properties of NFA films during film formation and can affect their charge transport properties. UV-Vis absorption measurements were carried out to determine the optical properties of small-molecule NFA films. Fig. 2a and b show the UV-Vis absorbance spectra of *o*-IDTBR- and L8-BO-based films processed using different solvents. The reference *o*-IDTBR films exhibit absorbance spectra with two main peaks at ∼414 and 735 nm. The reference L8-BO films also possess two main peaks in the absorbance spectra at ∼342 and 826 nm. As depicted in Fig. 2a, we observed blue shifts in the UV-Vis peak (735 nm) of the *o*-IDTBR films when processed using different solvents. Relative to the reference *o*-IDTBR film, layers processed from mesitylene and *o*-xylene solutions exhibit the largest blue shift in their absorption peaks. The blue-shifted spectra also manifest as colour changes in *o*-IDTBR solutions dissolved in mesitylene and *o*-xylene. These changes indicate the existence of intermolecular interactions, the strength of which depends on the solvent used.

Fig. 2c shows the Tauc plot (extracted from Fig. S3a, ESI†) of *o*-IDTBR films deposited from the different solvents. The analysis reveals small changes in the bandgap of each layer. Films cast from mesitylene and toluene exhibit the highest and the lowest bandgap, respectively. Moreover, the blue shift of the main absorption peak of the *o*-IDTBR films indicates changes in their molecular packing and, hence, crystallinity and morphology.[43,44]

In contrast to the *o*-IDTBR films, we did not observe any blue shift in the main absorption peak of the L8-BO films deposited from the same solvents (Fig. 2b). Instead, we observed a broadening of the main absorption peak at ∼826 nm in the L8-BO films processed from toluene and *o*-xylene relative to the reference L8-BO film. Meanwhile, the films processed by anisole and mesitylene experience a characteristic narrowing of the main absorption peaks. The difference in the absorption features of L8-BO films cast from different solvents also suggests differences in their electronic properties (including electronic, vibrational, and rotational energy levels).[45] The optical bandgap analysis of L8-BO films deposited from the different solvents is presented in Fig. 2d (extracted from Fig. S3b, ESI†).

Compared to reference L8-BO film, the broadening of the main absorption peak of L8-BO films cast from toluene and *o*-xylene is believed to originate from the different crystallisation motifs and the associated changes in the density of energy states.[46] Conversely, L8-BO films prepared from anisole and

mesitylene exhibit slightly larger optical bandgaps than the reference L8-BO film, which can be attributed to the stronger intermolecular interactions. These results demonstrate that using different solvents can lead to solid films with different microstructural, optical and electronic characteristics for both NFAs investigated.

To assess the impact of the different solvents on the charge transport properties of the NFA films, we fabricated TFTs using a top-gate and bottom-contact configuration. Devices were fabricated by evaporating a 35 nm-thin Au layer atop a 5 nm-thin Al adhesion layer on glass substrates to form the bottom source and drain (S–D) electrodes. To improve electron injection from Au to the small-molecule NFAs, we treated the Au films with polyethyleneimine (PEIE). Next, the NFA solutions were spun from various solvents and thermally annealed at 120 °C for *o*-IDTBR and 220 °C for L8-BO for 5 min inside a nitrogen-filled glovebox. Cytop was used as the gate dielectric owing to its hydroxyl-free nature.[47,48] Device fabrication was completed with the evaporation of a 70 nm-thick Al gate electrode.

Fig. 3a and b show the $I_{DS}^{1/2}$–V_G and transfer characteristics measured in saturation regime for *o*-IDTBR TFTs processed from the different solvents. Reference TFTs based on *o*-IDTBR processed from chlorobenzene (CB) solutions are also shown in Fig. 3a and b (black line). The CB-cast devices exhibit clear electron accumulation (n-channel) with a current on/off ratio of $\sim 10^4$. Changing the solvent to a non-chlorinated one affects the transfer characteristics of the TFTs (Fig. 3a and b). Compared to *o*-IDTBR TFTs prepared from chlorobenzene, the currents for the NFA-based devices processed from anisole, mesitylene, and *o*-xylene solutions were consistently lower. Specifically, *o*-IDTBR TFTs processed from *o*-xylene solution exhibit the lowest channel currents among all devices. Interestingly, *o*-IDTBR TFTs processed from the toluene solution exhibited optimal performance with a current on/off ratio of 7.6×10^5 (Fig. 3b), a low threshold voltage of 4.4 V, and a clear saturation regime (Fig. S4, ESI†), indicating good operating transistors.

To obtain further insight into the charge carrier transport dynamics, we extracted the field-effect electron mobility (μ_e) in the saturation regime from the transfer curves in Fig. 3a using the gradual channel approximation model:

$$\mu_e = \frac{2L}{WC_i}\left(\frac{\partial I_D^{1/2}}{\partial V_G}\right)^2 \quad (1)$$

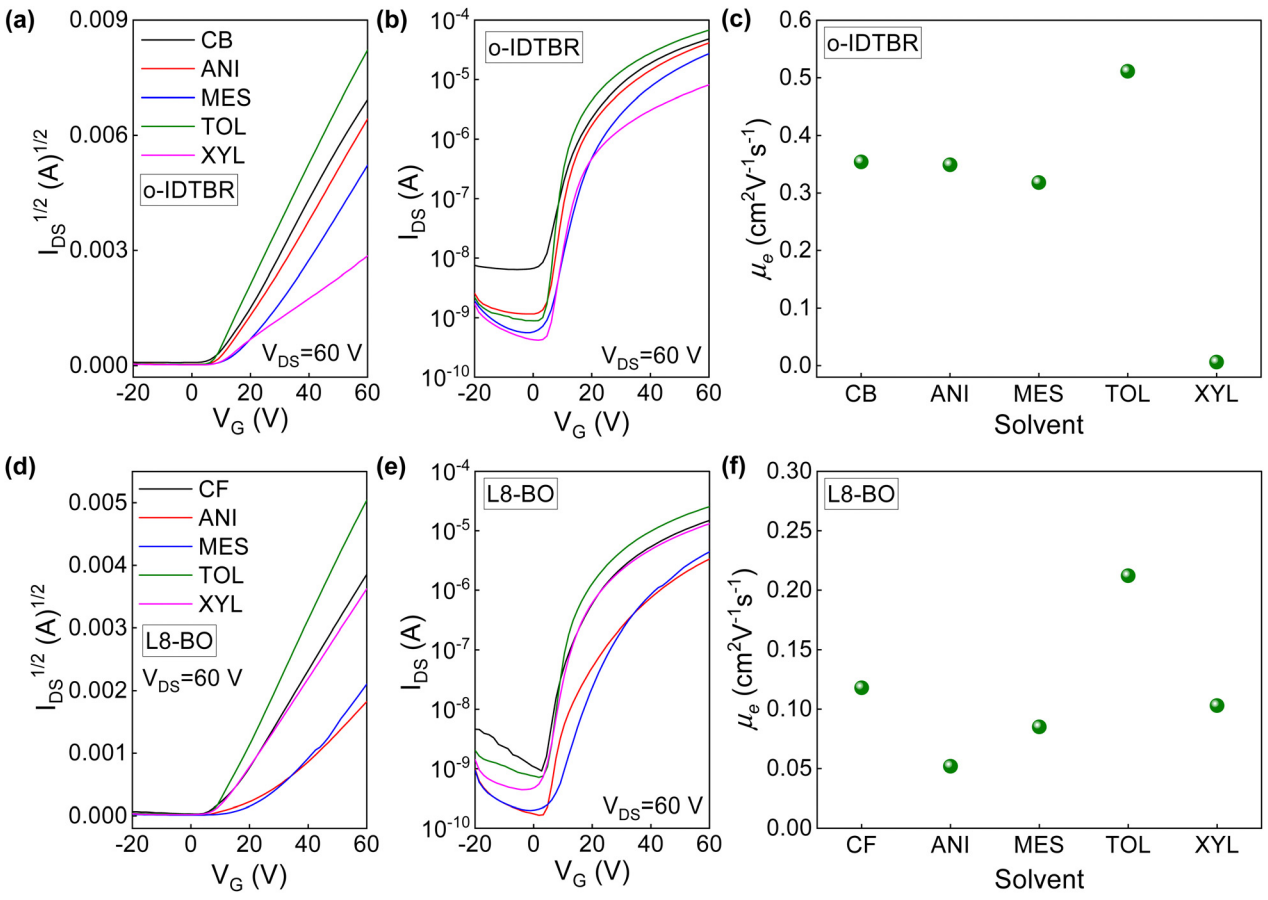

Fig. 3 (a) $I_{DS}^{1/2}$–V_G, (b) semi-logarithmic transfer characteristics, and (c) electron mobility at the saturation regime in *o*-IDTBR TFTs processed using different solvents. (d) $I_{DS}^{1/2}$–V_G, (e) semi-logarithmic transfer characteristics, and (f) electron mobility at the saturation regime in L8-BO TFTs processed using different solvents. The applied gate voltages (V_G) in the transfer characteristics are from −20 to 60 V, with a source–drain voltage (V_{DS}) of 60 V. The channel length and width of the devices are 30 and 1000 μm, respectively.

Here, L, W, C_i, I_D, and V_G denote the channel length, channel width, gate dielectric capacitance, source–drain current, and gate voltage, respectively. Table S1 (ESI†) summarises the operating parameters of transistors prepared from the different solvents, including electron mobility, on/off current ratio, and threshold voltage. Fig. 3c shows the electron mobility in *o*-IDTBR TFTs processed from the various solvents. *o*-IDTBR TFTs fabricated from chlorobenzene solution exhibited an electron mobility of 0.35 $cm^2\ V^{-1}\ s^{-1}$, consistent with previous reports.[49,50] The *o*-IDTBR TFTs processed from anisole and mesitylene possess electron mobility comparable to that cast from chlorobenzene solution. *o*-IDTBR TFTs processed from *o*-xylene show the lowest μ_e of 0.006 $cm^2\ V^{-1}\ s^{-1}$. On the other hand, *o*-IDTBR devices processed from toluene solution exhibit the μ_e of 0.56 $cm^2\ V^{-1}\ s^{-1}$, which is higher than that measured from TFTs processed from chlorobenzene.

Next, TFTs based on L8-BO films, processed from different solvents, were studied. L8-BO TFTs fabricated from a chloroform solution exhibited clear n-type current modulation with an on/off ratio of approximately 10^4 (Fig. 3d, e and Table S1, ESI†). Like *o*-IDTBR TFTs, dissolving L8-BO in different solvents affects the charge transport properties of the ensuing transistors (Fig. 3d and e). TFTs prepared from anisole and mesitylene exhibit significantly reduced channel current, an effect most likely attributed to the microstructure changes within the channel. L8-BO TFTs prepared from *o*-xylene solution show transfer characteristics comparable to those of the reference devices. In line with the *o*-IDTBR TFTs, the L8-BO devices processed from toluene exhibit optimum performance. The TFTs show improved current on/off ratios, reduced threshold voltage, and clear saturation profiles in their output characteristics, as shown in Fig. 3e and Table S1, Fig. S5 (ESI†), respectively.

The μ_e values for the L8-BO TFTs prepared from the different solvents are shown in Fig. 3f and Table S1 (ESI†). The reference devices exhibit a maximum electron mobility of 0.11 $cm^2\ V^{-1}\ s^{-1}$. Upon dissolving L8-BO in anisole and mesitylene, we found that the electron mobility decreases to 0.05 and 0.085 $cm^2\ V^{-1}\ s^{-1}$, respectively. L8-BO TFTs processed from *o*-xylene solution showed electron mobility similar to the reference TFTs processed from chloroform. Switching to toluene as the solvent leads to L8-BO TFTs with higher μ_e by almost a factor of two (up to 0.21 $cm^2\ V^{-1}\ s^{-1}$) compared to reference devices. These results reveal that solvent engineering is a promising and simple method for modulating electron transport in NFA-based TFTs.

To study the origin of the electron transport differences in NFA-based TFTs processed from different solvents, we conducted two-dimensional grazing incident wide angle X-ray scattering (2D-GIWAXS) measurements. Fig. 4a shows the 2D-GWAXS patterns of *o*-IDTBR NFA films cast using different solvents. The reference *o*-IDTBR NFA films processed from chlorobenzene solution exhibit strong peaks in the in-plane direction, consistent with the literature.[50] For films cast from anisole and mesitylene solutions, we observed that the GIWAXS pattern's intensities were reduced compared to the reference samples. Further suppression in the GIWAXS intensity is observed in *o*-IDTBR films cast from *o*-xylene, indicating a reduced film crystallinity. The latter explains the inferior charge transport in *o*-IDTBR TFTs processed from *o*-xylene. For *o*-IDTBR films processed from toluene, we observe more intense diffraction patterns in the in-plane and out-of-plane directions, indicating improved layer crystallinity. Strong in-plane and out-of-plane molecular packing is better illustrated in the corresponding line cuts shown in Figs. S6a and b (ESI†). Such features indicate three-dimensional (3D) packing, which can support 3D electron transport and is most likely the origin of the higher electron mobility measured in *o*-IDTBR TFTs processed from toluene (Fig. 3c).

We carried out 2D-GIWAXS measurements on the L8-BO films processed from the different solvents (Fig. 4b). L8-BO layers spun from chloroform exhibit visible peaks in the in-plane and out-of-plane directions. For films processed from anisole and mesitylene, the intensity of some of these diffraction peaks reduces significantly, indicating a lower crystallinity. The observation also explains the suppressed electron transport measured for L8-BO TFTs processed from anisole and mesitylene (Fig. 3d–f). In L8-BO films cast from *o*-xylene solution, the

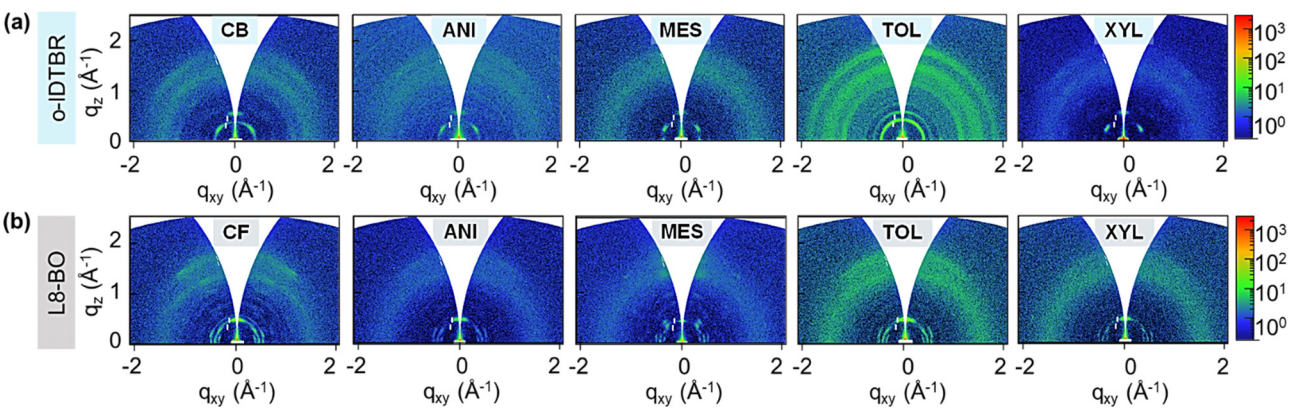

Fig. 4 Two-dimensional grazing incident wide angle X-ray scattering (2D-GIWAXS) spectra of (a) *o*-IDTBR and (b) L8-BO films processed from different solvents.

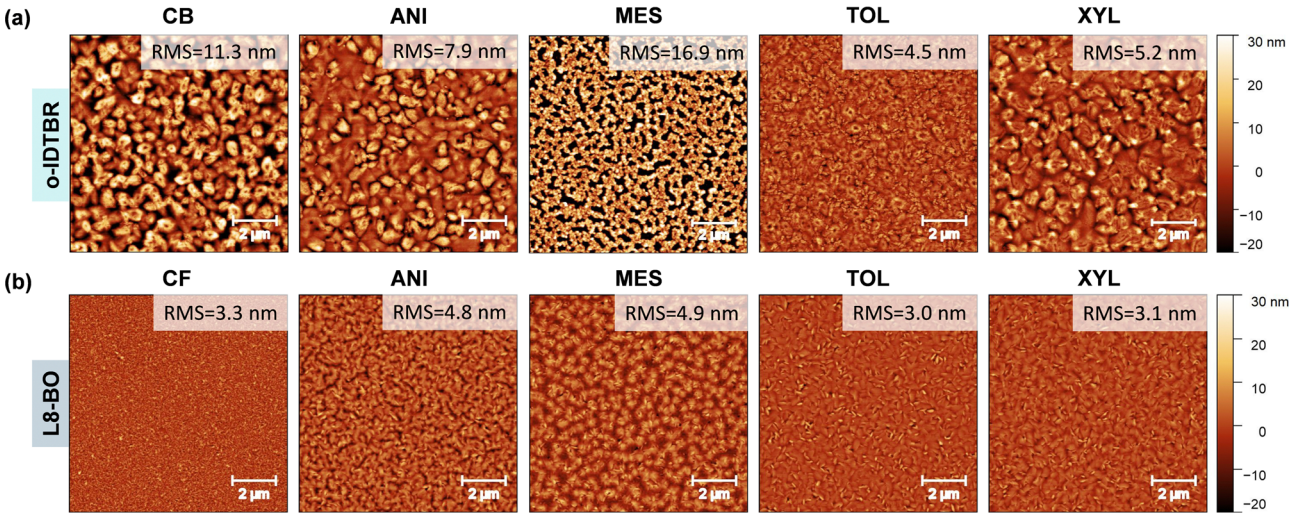

Fig. 5 Atomic force microscopy (AFM) images of (a) *o*-IDTBR and (b) L8-BO films processed using different solvents.

GIWAXS intensities appear comparable to those in the reference films, consistent with the transistor characterisation. Like *o*-IDTBR films, L8-BO layers processed from toluene exhibit a notably improved crystallinity (intense diffraction peaks, Fig. S6c and d, ESI†), highlighting toluene's efficacy as a solvent for NFA-based systems.

To gain further insights into the morphological properties of NFA films, we carried out atomic force microscopy (AFM) measurements. The AFM topography images of *o*-IDTBR films processed from different solvents are presented in Fig. 5a. The layer exhibits visible domains of varying sizes, which agrees with the literature.[50] The detailed domain features measured over a smaller scanning area are presented in Fig. S8a (ESI†). *o*-IDTBR films processed from anisole show smoother morphology than the reference *o*-IDTBR film. The latter feature indicates the formation of more amorphous films and can be responsible for the inferior charge transport observed (Fig. 3a–c). On the other hand, the mesitylene-processed *o*-IDTBR layer appears non-uniform with many disconnected domains and grain boundaries (Fig. 5a). The latter feature is believed to be responsible for the lower electron mobility of mesitylene-processed *o*-IDTBR TFTs (Fig. 3c). *o*-IDTBR films cast from *o*-xylene also exhibit a smoother morphology, but electron transport remains inferior due to the reduced layer crystallinity, as revealed by the GIWAXS measurements in Fig. 4a. *o*-IDTBR films spun from toluene appear continuous and smooth, as indicated by the narrow surface height distribution histograms in Fig. S7a and S11a (ESI†). Additional data on the film morphology measured for different scanning areas are presented in Fig. S8a and S10a (ESI†).

AFM images of L8-BO films prepared from various solvents are shown in Fig. 5b. AFM images obtained at scanning areas of 5 and 20 μm are shown in Fig. S8b and S10b (ESI†). The L8-BO films processed from chloroform show continuous topography with no visible cracks. On the other hand, L8-BO films processed from anisole and mesitylene solutions appear less continuous than the reference films, which explains the lower electron field-effect mobility (Fig. 3f). L8-BO films processed from *o*-xylene show improved film morphology compared to layers prepared from anisole and mesitylene solutions. Surprisingly, the electron mobility remains similar to that measured for the reference L8-BO TFTs (Fig. 3f). Like *o*-IDTBR, L8-BO films processed from toluene show improved layer morphology characterised by larger-size domains. These features are believed to be responsible for the highest electron mobility measured for *o*-IDTBR and L8-BO TFTs processed from toluene, among all other solvents studied. The results demonstrate that solvent engineering using non-chlorinated solvents provides a simple route to improving charge transport in technology-relevant small-molecule organic semiconductors. Moreover, it demonstrates the possibility of realising well-performing NFA-based optoelectronics from less toxic solvents.

Conclusions

We have successfully demonstrated NFA-based TFTs processed from various non-chlorinated solvents. A strong relation was established between the solvent used and the electron-transporting properties of the ensuing NFA-based transistors. The electron mobility in both *o*-IDTBR and L8-BO transistors could be significantly increased by using non-chlorinated solvents. The enhanced electron transport was shown to originate from the layers' improved crystallinity, highlighting the tremendous promise of this simple solvent-engineering approach. Our findings provide valuable insights towards the facile and cost-effective fabrication of high-performance NFA-based (opto)electronic devices using more environmentally benign solvents.

Conflicts of interest

There are no conflicts to declare.

Acknowledgements

This publication is based upon work supported by the King Abdullah University of Science and Technology (KAUST) Office of Sponsored Research (OSR) under Award No: OSR-2018-CARF/CCF-3079, and OSR-2019-CRG8-4095. The authors gratefully acknowledge the KAUST Core Lab facility and staff for their support and assistance in this work.

References

1 K. Leo, *Nat. Rev. Mater.*, 2016, **1**, 16056.
2 O. Ostroverkhova, *Chem. Rev.*, 2016, **116**, 13279–13412.
3 Y. Hu, J. Wang, C. Yan and P. Cheng, *Nat. Rev. Mater.*, 2022, **7**, 836–838.
4 L. Sun, K. Fukuda and T. Someya, *npj Flexible Electron.*, 2022, **6**, 1–14.
5 H. Ren, J.-D. Chen, Y.-Q. Li and J.-X. Tang, *Adv. Sci.*, 2021, **8**, 2002418.
6 J. Song, H. Lee, E. G. Jeong, K. C. Choi and S. Yoo, *Adv. Mater.*, 2020, **32**, 1907539.
7 S. Griggs, A. Marks, D. Meli, G. Rebetez, O. Bardagot, B. D. Paulsen, H. Chen, K. Weaver, M. I. Nugraha, E. A. Schafer, J. Tropp, C. M. Aitchison, T. D. Anthopoulos, N. Banerji, J. Rivnay and I. McCulloch, *Nat. Commun.*, 2022, **13**, 7964.
8 B. Wang, A. D. Scaccabarozzi, H. Wang, M. Koizumi, M. Insan Nugraha, Y. Lin, Y. Firdaus, Y. Wang, S. Lee, T. Yokota, T. D. Anthopoulos and T. Someya, *J. Mater. Chem. C*, 2021, **9**, 3129–3135.
9 S. E. Root, S. Savagatrup, A. D. Printz, D. Rodriquez and D. J. Lipomi, *Chem. Rev.*, 2017, **117**, 6467–6499.
10 H. T. Yi, M. M. Payne, J. E. Anthony and V. Podzorov, *Nat. Commun.*, 2012, **3**, 1259.
11 K. Liu, B. Ouyang, X. Guo, Y. Guo and Y. Liu, *npj Flexible Electron.*, 2022, **6**, 1–19.
12 M. Li, J. Zheng, X. Wang, R. Yu, Y. Wang, Y. Qiu, X. Cheng, G. Wang, G. Chen, K. Xie and J. Tang, *Nat. Commun.*, 2022, **13**, 4912.
13 T. Yang, J. S. Mehta, A. M. Haruk and J. M. Mativetsky, *J. Mater. Chem. C*, 2018, **6**, 2970–2977.
14 M. I. Nugraha, H. Matsui, S. Watanabe, T. Kubo, R. Häusermann, S. Z. Bisri, M. Sytnyk, W. Heiss, M. A. Loi and J. Takeya, *Adv. Electron. Mater.*, 2017, **3**, 1600360.
15 S. Chung, K. Cho and T. Lee, *Adv. Sci.*, 2019, **6**, 1801445.
16 A. Luczak, K. Y. Mitra, R. R. Baumann, R. Zichner, B. Luszczynska and J. Jung, *Sci. Rep.*, 2022, **12**, 10887.
17 W. Zhao, J. Ding, Y. Zou, C. Di and D. Zhu, *Chem. Soc. Rev.*, 2020, **49**, 7210–7228.
18 P. Kafourou, M. I. Nugraha, A. Nikitaras, L. Tan, Y. Firdaus, F. Aniés, F. Eisner, B. Ding, J. Wenzel, M. Holicky, L. Tsetseris, T. D. Anthopoulos and M. Heeney, *ACS Mater. Lett.*, 2022, **4**, 165–174.
19 J. Zhang, F. Bai, I. Angunawela, X. Xu, S. Luo, C. Li, G. Chai, H. Yu, Y. Chen, H. Hu, Z. Ma, H. Ade and H. Yan, *Adv. Energy Mater.*, 2021, **11**, 2102596.
20 P. Cheng, G. Li, X. Zhan and Y. Yang, *Nat. Photon*, 2018, **12**, 131–142.
21 Y. Lin, Y. Firdaus, M. I. Nugraha, F. Liu, S. Karuthedath, A.-H. Emwas, W. Zhang, A. Seitkhan, M. Neophytou, H. Faber, E. Yengel, I. McCulloch, L. Tsetseris, F. Laquai and T. D. Anthopoulos, *Adv. Sci.*, 2020, **7**, 1903419.
22 Y. Lin, M. I. Nugraha, Y. Firdaus, A. D. Scaccabarozzi, F. Aniés, A.-H. Emwas, E. Yengel, X. Zheng, J. Liu, W. Wahyudi, E. Yarali, H. Faber, O. M. Bakr, L. Tsetseris, M. Heeney and T. D. Anthopoulos, *ACS Energy Lett.*, 2020, **5**, 3663–3671.
23 Y. Lin, Y. Firdaus, F. H. Isikgor, M. I. Nugraha, E. Yengel, G. T. Harrison, R. Hallani, A. El-Labban, H. Faber, C. Ma, X. Zheng, A. Subbiah, C. T. Howells, O. M. Bakr, I. McCulloch, S. D. Wolf, L. Tsetseris and T. D. Anthopoulos, *ACS Energy Lett.*, 2020, **5**, 2935–2944.
24 Y. Firdaus, C. H. Y. Ho, Y. Lin, E. Yengel, V. M. Le Corre, M. I. Nugraha, E. Yarali, F. So and T. D. Anthopoulos, *ACS Energy Lett.*, 2020, **5**, 3692–3701.
25 J.-W. Liang, Y. Firdaus, R. Azmi, H. Faber, D. Kaltsas, C. H. Kang, M. I. Nugraha, E. Yengel, T. K. Ng, S. De Wolf, L. Tsetseris, B. S. Ooi and T. D. Anthopoulos, *ACS Energy Lett.*, 2022, **7**, 3139–3148.
26 C. M. Alder, J. D. Hayler, R. K. Henderson, A. M. Redman, L. Shukla, L. E. Shuster and H. F. Sneddon, *Green Chem.*, 2016, **18**, 3879–3890.
27 Y. Zhang, K. Liu, J. Huang, X. Xia, J. Cao, G. Zhao, P. W. K. Fong, Y. Zhu, F. Yan, Y. Yang, X. Lu and G. Li, *Nat. Commun.*, 2021, **12**, 4815.
28 Y.-Y. Yu, K.-Y. Shih, Y.-C. Peng, Y.-C. Chiu, C.-C. Kuo, C.-C. Yang and C.-P. Chen, *Mater. Chem. Phys.*, 2022, **282**, 125971.
29 D. Wang, G. Zhou, Y. Li, K. Yan, L. Zhan, H. Zhu, X. Lu, H. Chen and C.-Z. Li, *Adv. Funct. Mater.*, 2022, **32**, 2107827.
30 S. Strohm, F. Machui, S. Langner, P. Kubis, N. Gasparini, M. Salvador, I. McCulloch, H.-J. Egelhaaf and C. J. Brabec, *Energy Environ. Sci.*, 2018, **11**, 2225–2234.
31 N. Li, I. McCulloch and C. J. Brabec, *Energy Environ. Sci.*, 2018, **11**, 1355–1361.
32 N. Gasparini, A. Wadsworth, M. Moser, D. Baran, I. McCulloch and C. J. Brabec, *Adv. Energy Mater.*, 2018, **8**, 1703298.
33 C. Li, J. Zhou, J. Song, J. Xu, H. Zhang, X. Zhang, J. Guo, L. Zhu, D. Wei, G. Han, J. Min, Y. Zhang, Z. Xie, Y. Yi, H. Yan, F. Gao, F. Liu and Y. Sun, *Nat. Energy*, 2021, **6**, 605–613.
34 A. F. Paterson, R. Li, A. Markina, L. Tsetseris, S. MacPhee, H. Faber, A.-H. Emwas, J. Panidi, H. Bristow, A. Wadsworth, D. Baran, D. Andrienko, M. Heeney, I. McCulloch and T. D. Anthopoulos, *J. Mater. Chem. C*, 2021, **9**, 4486–4495.
35 H. Bristow, K. J. Thorley, A. J. P. White, A. Wadsworth, M. Babics, Z. Hamid, W. Zhang, A. F. Paterson, J. Kosco, J. Panidi, T. D. Anthopoulos and I. McCulloch, *Adv. Electron. Mater.*, 2019, **5**, 1900344.
36 J. Gao, N. Yu, Z. Chen, Y. Wei, C. Li, T. Liu, X. Gu, J. Zhang, Z. Wei, Z. Tang, X. Hao, F. Zhang, X. Zhang and H. Huang, *Adv. Sci.*, 2022, **9**, 2203606.

37 C. Li, X. Gu, Z. Chen, X. Han, N. Yu, Y. Wei, J. Gao, H. Chen, M. Zhang, A. Wang, J. Zhang, Z. Wei, Q. Peng, Z. Tang, X. Hao, X. Zhang and H. Huang, *J. Am. Chem. Soc.*, 2022, **144**, 14731–14739.
38 J. Song, L. Zhu, C. Li, J. Xu, H. Wu, X. Zhang, Y. Zhang, Z. Tang, F. Liu and Y. Sun, *Matter*, 2021, **4**, 2542–2552.
39 D. Li, N. Deng, Y. Fu, C. Guo, B. Zhou, L. Wang, J. Zhou, D. Liu, W. Li, K. Wang, Y. Sun and T. Wang, *Adv. Mater.*, 2023, **35**, 2208211.
40 L. Zhu, M. Zhang, J. Xu, C. Li, J. Yan, G. Zhou, W. Zhong, T. Hao, J. Song, X. Xue, Z. Zhou, R. Zeng, H. Zhu, C.-C. Chen, R. C. I. MacKenzie, Y. Zou, J. Nelson, Y. Zhang, Y. Sun and F. Liu, *Nat. Mater.*, 2022, **21**, 656–663.
41 K. An, W. Zhong, F. Peng, W. Deng, Y. Shang, H. Quan, H. Qiu, C. Wang, F. Liu, H. Wu, N. Li, F. Huang and L. Ying, *Nat. Commun.*, 2023, **14**, 2688.
42 A. A. Virkar, S. Mannsfeld, Z. Bao and N. Stingelin, *Adv. Mater.*, 2010, **22**, 3857–3875.
43 H. Chen, D. Hu, Q. Yang, J. Gao, J. Fu, K. Yang, H. He, S. Chen, Z. Kan, T. Duan, C. Yang, J. Ouyang, Z. Xiao, K. Sun and S. Lu, *Joule*, 2019, **3**, 3034–3047.
44 Q. Liang, X. Jiao, Y. Yan, Z. Xie, G. Lu, J. Liu and Y. Han, *Adv. Funct. Mater.*, 2019, **29**, 1807591.
45 L. Krückemeier, P. Kaienburg, J. Flohre, K. Bittkau, I. Zonno, B. Krogmeier and T. Kirchartz, *Commun. Phys.*, 2018, **1**, 1–10.
46 N. Zarrabi, O. J. Sandberg, P. Meredith and A. Armin, *J. Phys. Chem. Lett.*, 2023, **14**, 3174–3185.
47 M. I. Nugraha, E. Yarali, Y. Firdaus, Y. Lin, A. El-Labban, M. Gedda, E. Lidorikis, E. Yengel, H. Faber and T. D. Anthopoulos, *ACS Appl. Mater. Interfaces*, 2020, **12**, 31591–31600.
48 M. I. Nugraha, R. Häusermann, S. Watanabe, H. Matsui, M. Sytnyk, W. Heiss, J. Takeya and M. A. Loi, *ACS Appl. Mater. Interfaces*, 2017, **9**, 4719–4724.
49 F. Aniés, M. I. Nugraha, A. Fall, J. Panidi, Y. Zhao, P. Vanelle, L. Tsetseris, J. Broggi, T. D. Anthopoulos and M. Heeney, *Adv. Funct. Mater.*, 2023, **33**, 2212305.
50 M. I. Nugraha, M. Gedda, Y. Firdaus, A. D. Scaccabarozzi, W. Zhang, S. Alshammari, F. Aniés, B. Adilbekova, A.-H. Emwas, I. McCulloch, M. Heeney, L. Tsetseris and T. D. Anthopoulos, *Adv. Funct. Mater.*, 2022, **32**, 2202954.

